FEATURE

Experimental implementation of linear and nonlinear control laws

Stabilization of a Mini Rotorcraft with Four Rotors

By Pedro Castillo, Rogelio Lozano, and Alejandro Dzul

Flight control of unmanned helicopters is an area that poses interesting problems for control researchers. The classical control strategy for helicopters assumes a linear model obtained for a particular operating point. Applying modern nonlinear control theory can improve the performance of the controller and enable the tracking of aggressive trajectories, as demonstrated in [1] for a 5-ft diameter main rotor helicopter.

Civil and military applications of autonomous flying vehicles have been steadily increasing over the last few years. Traffic surveillance, air pollution monitoring, area mapping, agricultural applications, and remote inspection require high maneuverability and robustness with respect to disturbances. Since rotary wing vehicles can take off and land in limited spaces and hover above targets, these vehicles have certain advantages over conventional fixed-wing aircraft for surveillance and inspection tasks.

1066-033X/05/$20.00©2005IEEE

The quad rotor is an excellent flying vehicle for investigating issues in automatic control, advanced sensor technology, and computer science. Autonomous flight poses research challenges such as intelligent control of aerial robots, three-dimensional (3-D) trajectory planning, multivehicle air traffic management, and collision avoidance. Since the quad rotor is dynamically unstable, control algorithms are required for stabilization.

Applying modern nonlinear control theory can improve the performance of the controller and enable tracking of aggressive trajectories.

The classical helicopter consists of a main rotor and a tail rotor. Other types of helicopters include the twin rotor, or tandem helicopter, and the coaxial rotors, helicopters having two counter-rotating rotors on the same shaft. We are particularly interested in controlling the quad rotor, a helicopter having four rotors, as shown in Figure 1. The electric quad-rotor helicopter is mechanically simpler and easier to repair than a classical electric helicopter. Since the mini rotorcraft is easy to operate, this device serves as a convenient laboratory testbed for studying modern nonlinear control techniques. Commercially available quad-rotor helicopters, such as those manufactured by Draganfly and Intellicopter, have four electric motors. Quad-rotor helicopters using four combustion engines do not present any advantages compared to classical helicopters. At the current time, none are commercially available.

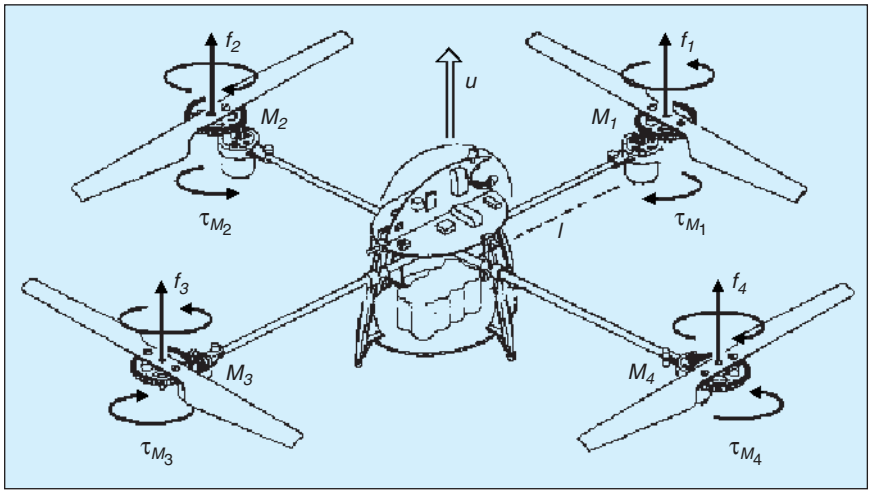

Figure 1. *The quad-rotor control inputs. The mini rotorcraft is controlled by varying the speeds of four electric motors. Each motor produces a thrust f_i, and these thrusts combine to generate the main thrust $u = \sum_{i=1}^{4} f_i$. The difference between the front rotor blade speed and the rear rotor blade speed produces a pitch torque. The roll torque is produced similarly. The yaw torque is the sum of the torques of each motor [see (1) and (2)].*

The quad-rotor control problem is similar to that of controlling a planar vertical takeoff and landing (PVTOL) aircraft, which evolves in a vertical plane [2]–[4]. The aircraft has three degrees of freedom, (x, y, θ), corresponding to its position in the plane and pitch angle. The PVTOL has two independent thrusters that produce a force and an angular momentum; it thus has three degrees of freedom and only two inputs. Hence, the PVTOL is underactuated.

Characteristics of the Quad Rotor

Conventional helicopters modify the lift force by varying the collective pitch of the rotor blades. These helicopters use a mechanical device known as a swashplate to change the pitch angle of the rotor blades in a cyclic manner so as to obtain the pitch and roll control torques of the vehicle. In contrast, the quad rotor does not have a swashplate, and it has constant pitch blades. A quad rotor is controlled by varying the angular speed of each rotor. The force f_i produced by motor i is proportional to the square of the angular speed, that is $f_i = k\omega_i^2$. Since each motor turns in a fixed direction, the produced force f_i is always positive (see Figure 1). The front and rear motors rotate counterclockwise, while the other two motors rotate clockwise. With this arrangement, gyroscopic effects and aerodynamic torques tend to cancel in trimmed flight. The main thrust is the sum of the individual thrusts of each motor (see Figure 1). The pitch torque is a function of the difference $f_1 - f_3$, the roll torque is a function of $f_2 - f_4$, and the yaw torque is the sum $\tau_{M_1} + \tau_{M_2} + \tau_{M_3} + \tau_{M_4}$, where τ_{M_i} is the reaction torque of motor i due to shaft acceleration and the blade's drag. Using Newton's second law and neglecting shaft friction, we have

$$I_M \dot{\omega}_i = -b\,\omega_i^2 + \tau_{M_i},$$

where I_M is the angular momentum of the ith motor and $b > 0$ is a constant.

A quad rotor moves forward by pitching. This motion is obtained by increasing the speed of the rear motor M_3 while reducing the speed of the front motor M_1. Likewise, roll motion

is obtained using the lateral motors. Yaw motion is obtained by increasing the torque of the front and rear motors, τ_{M_1} and τ_{M_3}, respectively, while decreasing the torque of the lateral motors, τ_{M_2} and τ_{M_4}. These motions can be accomplished while keeping the total thrust $u = f_1 + f_2 + f_3 + f_4$ constant. In steady state, that is, when $\dot{\omega}_i = 0$, the yaw torque is

$$\tau_\psi = b\left(\omega_1^2 + \omega_3^2 - \omega_2^2 - \omega_4^2\right), \tag{1}$$

and the main thrust is

$$u = k\sum_{i=1}^{4} \omega_i^2. \tag{2}$$

In view of its configuration, the quad rotor shares some similarities with the PVTOL aircraft. Indeed, if the roll or pitch and yaw angles are set to zero, the quad rotor reduces to a PVTOL and can be viewed as two PVTOLs connected with orthogonal axes.

In this article, we first model the dynamics of the quad rotor. Then we propose a control strategy by viewing the aircraft as the interconnection of two PVTOLs. The control algorithm is based on the nested saturation control strategy introduced in [5]. Using computer simulations, we compare the performance of the nonlinear control algorithm with an linear quadratic regulator (LQR) control law. The controller is implemented on a PC, and we present the results of laboratory experiments. Finally, we present some conclusions.

Dynamical Model

In this section, we derive a dynamical model of the quad rotor. This model is obtained by representing the aircraft as a rigid body evolving in a 3-D space due to the main thrust and three torques. The main thrust u is shown in Figure 1. The dynamics of the four electric motors are fast and, thus, are neglected.

The generalized coordinates of the rotorcraft are

$$q = (x, y, z, \psi, \theta, \phi) \in \mathbb{R}^6,$$

where $\xi = (x, y, z) \in \mathbb{R}^3$ denotes the position of the center of mass of the helicopter relative to a fixed inertial frame $\mathcal{I}$, and $\eta = (\psi, \theta, \phi) \in \mathbb{R}^3$ are the Euler angles, ψ is the yaw angle around the z-axis, θ is the pitch angle around the modified y-axis, and ϕ is the roll angle around the modified x-axis [6]–[8], which represent the orientation of the rotorcraft.

Define the Lagrangian

$$L(q, \dot{q}) = T_{\text{trans}} + T_{\text{rot}} - U,$$

where $T_{\text{trans}} = (m/2)\dot{\xi}^T\dot{\xi}$ is the translational kinetic energy, $T_{\text{rot}} = (1/2)\omega^T\mathbf{I}\,\omega$ is the rotational kinetic energy, $U = mgz$ is the potential energy, z is the rotorcraft altitude, m is the mass of the quad rotor, ω is the angular velocity, $\mathbf{I}$ is the inertia matrix, and g is the acceleration due to gravity. The angular velocity vector ω resolved in the body fixed frame is related to the generalized velocities $\dot{\eta}$ (in the region where the Euler angles are valid) by means of the kinematic relationship [9]

$$\dot{\eta} = W_v^{-1}\omega,$$

where

$$W_v = \begin{bmatrix} -\sin\theta & 0 & 1 \\ \cos\theta\sin\psi & \cos\psi & 0 \\ \cos\theta\cos\psi & -\sin\psi & 0 \end{bmatrix}.$$

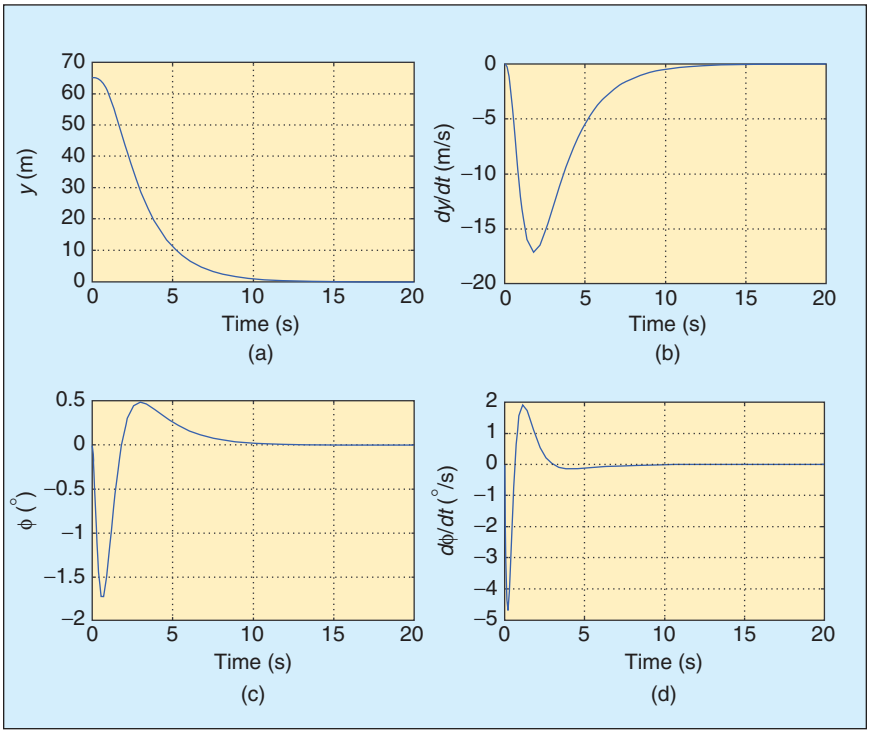

Figure 2. *Simulation of the LQR control law applied to the linear system (22). The initial conditions are altitude $y(0) = 70$ m and roll $\phi(0) = 0°$. In this case, y and ϕ converge to zero as expected.*

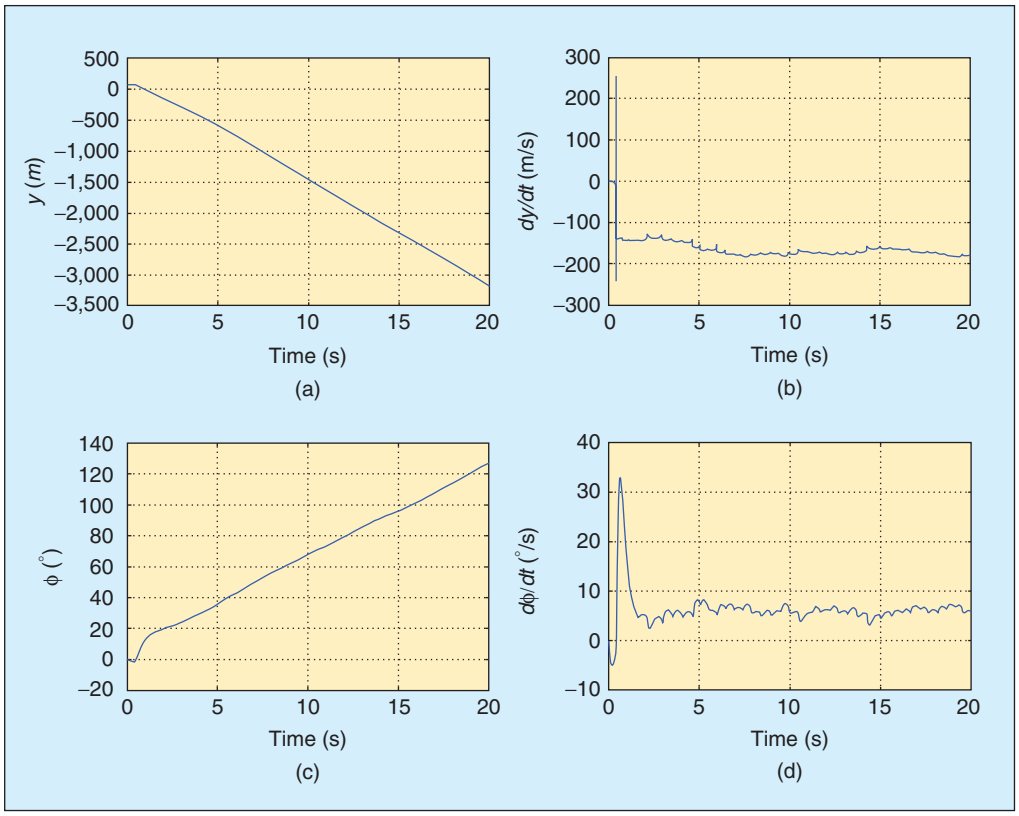

Figure 3. *Simulation of the LQR control law applied to the nonlinear subsystem (10) and (15). The initial conditions are $y(0) = 70$ m and $\phi(0) = 0^\circ$. Both y and ϕ diverge when the LQR controller is applied to the nonlinear subsystem (10) and (15). Therefore, the stability of the closed-loop system is not global, and the initial condition considered is outside of the domain of attraction.*

Define

$$\mathbb{J} = \mathbb{J}(\eta) = W_v^T \mathbf{I}\, W_v,$$

so that

$$T_{\text{rot}} = \frac{1}{2}\dot{\eta}^T \mathbb{J}\dot{\eta}.$$

Thus, the matrix $\mathbb{J} = \mathbb{J}(\eta)$ acts as the inertia matrix for the full rotational kinetic energy of the helicopter expressed in terms of the generalized coordinates η.

The model of the full rotorcraft dynamics is obtained from Euler-Lagrange equations with external generalized forces

$$\frac{d}{dt}\frac{\partial \mathcal{L}}{\partial \dot{q}} - \frac{\partial \mathcal{L}}{\partial q} = \begin{bmatrix} F_\xi \\ \tau \end{bmatrix},$$

where $F_\xi = R\widehat{F} \in \mathbb{R}^3$ is the translational force applied to the rotorcraft due to main thrust, $\tau \in \mathbb{R}^3$ represents the yaw, pitch, and roll moments, and R denotes the rotational matrix $R(\psi, \theta, \phi) \in SO(3)$ representing the orientation of the aircraft relative to a fixed inertial frame. From Figure 1, it follows that

$$\widehat{F} = \begin{bmatrix} 0 \\ 0 \\ u \end{bmatrix},$$

where u is the main thrust directed out the top of the aircraft expressed as

$$u = \sum_{i=1}^{4} f_i,$$

and, for $i = 1, \ldots, 4$, f_i is the force produced by motor M_i, as shown in Figure 1. Typically, $f_i = k\omega_i^2$, where k is a constant and ω_i is the angular speed of the ith motor. We assume that the center of gravity is located at the intersection of the line joining motors M_1 and M_3 and the line joining motors M_2 and M_4 (see Figure 1). The generalized torques are thus

Table 1. Parameter values used in the nonlinear control laws (16), (17), (20), and (21). These parameters are manually tuned to improve the performance of the closed-loop system.

Control parameter	Value
a_{z_1}	0.001
a_{z_2}	0.002
a_{ψ_1}	2.374
a_{ψ_2}	0.08
b_{ϕ_1}	2
b_{ϕ_2}	1
b_{ϕ_3}	0.2
b_{ϕ_4}	0.1
b_{θ_1}	2
b_{θ_2}	1
b_{θ_3}	0.2
b_{θ_4}	0.1
T	17 ms
ms	

$$\tau = \begin{bmatrix} \tau_\psi \\ \tau_\theta \\ \tau_\phi \end{bmatrix} \triangleq \begin{bmatrix} \sum_{i=1}^{4} \tau_{M_i} \\ (f_2 - f_4)\ell \\ (f_3 - f_1)\ell \end{bmatrix},$$

where ℓ is the distance between the motors and the center of gravity, and τ_{M_i} is the moment produced by motor M_i, $i = 1, \ldots, 4$, around the center of gravity of the aircraft.

Thus, we obtain

$$m\ddot{\xi} + \begin{pmatrix} 0 \\ 0 \\ mg \end{pmatrix} = F_\xi = R\widehat{F}, \tag{3}$$

$$\mathbb{J}\ddot{\eta} + C(\eta, \dot{\eta})\dot{\eta} = \tau, \tag{4}$$

where

$$C(\eta, \dot{\eta}) = \dot{\mathbb{J}} - \frac{1}{2}\frac{\partial}{\partial \eta}(\dot{\eta}^T \mathbb{J})$$

is the Coriolis term, which contains the gyroscopic and centrifugal terms associated with the η dependence of $\mathbb{J}$.

Finally, we obtain from (3) and (4)

$$m\ddot{x} = -u\sin\theta, \tag{5}$$

$$m\ddot{y} = u\cos\theta\sin\phi, \tag{6}$$

$$m\ddot{z} = u\cos\theta\cos\phi - mg, \tag{7}$$

$$\ddot{\psi} = \tilde{\tau}_\psi, \tag{8}$$

$$\ddot{\theta} = \tilde{\tau}_\theta, \tag{9}$$

$$\ddot{\phi} = \tilde{\tau}_\phi, \tag{10}$$

where x and y are coordinates in the horizontal plane, z is the vertical position, and $\tilde{\tau}_\psi$, $\tilde{\tau}_\theta$, and $\tilde{\tau}_\phi$ are the yawing moment, pitching moment, and rolling moment, respectively. These moments are related to the generalized torques τ_ψ, τ_θ, τ_ϕ by

$$\tilde{\tau} = \begin{bmatrix} \tilde{\tau}_\psi \\ \tilde{\tau}_\theta \\ \tilde{\tau}_\phi \end{bmatrix} = \mathrm{J}^{-1}(\tau - C(\eta, \dot{\eta})\dot{\eta}).$$

Control Strategy

In this section, we develop a control strategy for stabilizing the quad rotor at hover. The controller synthesis procedure regulates each state sequentially using a priority rule as follows. We first use the main thrust u to stabilize the altitude

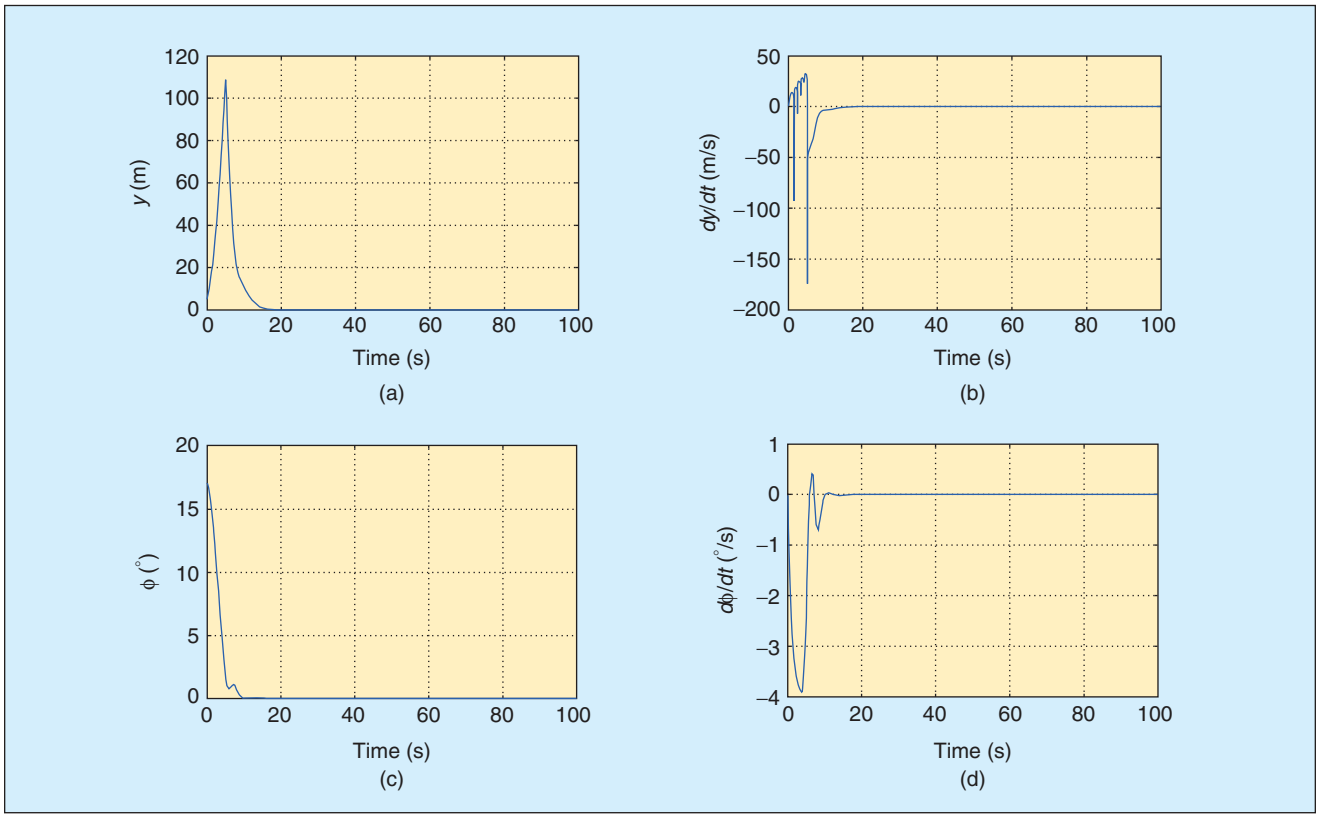

Figure 4. *Simulation of the nonlinear control law (20) with the nonlinear subsystem (10) and (15). The initial conditions are $y(0) = 5$ m, $\dot{y}(0) = 0$ m/s, $\dot{\phi}(0) = 0°/s$, and $\phi(0) = 17°$. The states y, $\dot{y}$, ϕ, $\dot{\phi}$ converge to zero despite the fact that the initial condition $\phi(0)$ is far from the origin.*

of the rotorcraft. Next, we stabilize the yaw angle. We then control the roll angle ϕ and the y displacement using a controller designed for the PVTOL model [2], [10]. Finally, the pitch angle θ and the x displacement are controlled.

The proposed control strategy is simple to implement and easy to tune. The experimental setup is such that the four control inputs can independently operate in either manual or automatic modes. For flight safety reasons, this feature is helpful for implementing the control strategy. The quad-rotor helicopter can be operated in semi-automatic mode, in which the remote pilot commands only the altitude and the desired position, leaving the orientation stabilization task to the control law.

Control of Altitude and Yaw

The vertical displacement z in (7) is controlled by forcing the altitude to satisfy the dynamics of a linear system. Thus, we set

$$u = (r_1 + mg)\frac{1}{\cos\theta\cos\phi}, \tag{11}$$

where r_1 is given by the proportional derivative (PD) controller

$$r_1 \triangleq -a_{z_1}\dot{z} - a_{z_2}(z - z_d), \tag{12}$$

where a_{z_1} and a_{z_2} are positive constants and z_d is a positive constant representing the desired altitude. To control yaw angle, we set

$$\tilde{\tau}_\psi = -a_{\psi_1}\dot{\psi} - a_{\psi_2}(\psi - \psi_d). \tag{13}$$

Introducing (11)–(13) into (5)–(8) and assuming $\cos\theta\cos\phi \neq 0$, that is, $\theta, \phi \in (-\pi/2, \pi/2)$, we obtain

$$m\ddot{x} = -(r_1 + mg)\frac{\tan\theta}{\cos\phi}, \tag{14}$$

$$m\ddot{y} = (r_1 + mg)\tan\phi, \tag{15}$$

$$\ddot{z} = \frac{1}{m}\left(-a_{z_1}\dot{z} - a_{z_2}(z - z_d)\right), \tag{16}$$

$$\ddot{\psi} = -a_{\psi_1}\dot{\psi} - a_{\psi_2}(\psi - \psi_d). \tag{17}$$

The control gains a_{ψ_1}, a_{ψ_2}, a_{z_1},and a_{z_2} are positive constants chosen to ensure stable, well-damped response of the quad rotor. From (16) and (17) it follows that, if ψ_d and z_d are constants, then ψ and z converge. Therefore, $\dot{\psi}$ and $\ddot{\psi} \to 0$, which, using (17), implies that $\psi \to \psi_d$. Similarly, $z \to z_d$.

Control of Lateral Position and Roll

We now determine the input $\tilde{\tau}_\phi$ such that y and ϕ, in (10) and (15), converge to zero. We assume $\psi_d \equiv 0$ in (13) and (17). Therefore, from (17) it follows that $\psi \to 0$. Note that (12) and (16) imply that $r_1 \to 0$.

Since the quad-rotor control inputs are subject to amplitude physical constraints,

$$\begin{aligned} 0 < u < 4\ V,\\ |\tilde{\tau}_\psi| \leq 2\ V,\\ |\tilde{\tau}_\theta| \leq 2\ V,\\ |\tilde{\tau}_\phi| \leq 2\ V, \end{aligned}$$

we use the control strategy developed in [5]. The nested saturation technique developed in [5] can exponentially stabilize a chain of integrators with bounded input. The amplitudes of the saturation functions can be chosen in such a way that, after a finite time T', the roll angle lies in the interval $-1\ \text{rad} \leq \phi \leq 1\ \text{rad}$. Therefore, for $t > T'$ $|\tan\phi - \phi| < 0.54$. Thus, after sufficient time, r_1 is small and the (y, ϕ) subsystem reduces to

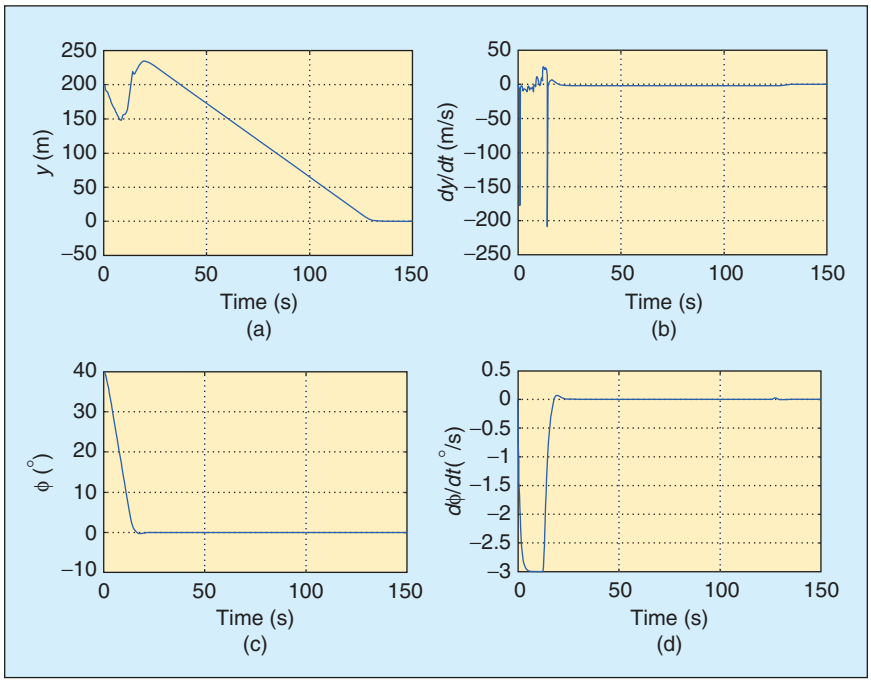

Figure 5. *Simulation of the nonlinear control law with the nonlinear subsystem (10) and (15). The initial conditions are $y(0) = 200$ m, $\dot{y}(0) = 0$ m/s, $\dot{\phi}(0) = 0°$/s, and $\phi(0) = 40°$. These values are chosen to show that the states $(y, \dot{y}, \phi, \dot{\phi})$ converge to zero when the initial roll angular displacement and y position are very far from the origin. Notice that the control strategy first brings the roll angle ϕ close to zero and then carries the y position to the origin.*

$$\ddot{y} = g\phi, \tag{18}$$
$$\ddot{\phi} = \tilde{\tau}_\phi, \tag{19}$$

which represents four integrators in cascade.

For (18)–(19), the nested saturation controller has the form

$$\tilde{\tau}_\phi = -\sigma_{\phi_1}\left(\dot{\phi} + \sigma_{\phi_2}\left(\phi + \dot{\phi} + \sigma_{\phi_3}\left(2\phi + \dot{\phi} + \frac{\dot{y}}{g} + \sigma_{\phi_4}\left(\dot{\phi} + 3\phi + 3\frac{\dot{y}}{g} + \frac{y}{g}\right)\right)\right)\right), \tag{20}$$

where σ_a is a saturation function of the form

$$\sigma_a(s) = \begin{cases} -a & s < -a, \\ s & -a \le s \le a, \\ a & s > a. \end{cases}$$

The closed loop is asymptotically stable (see [5]), and therefore ϕ, $\dot{\phi}$, y, and $\dot{y}$ converge to zero.

Control of Forward Position and Pitch

For small ϕ and r_1, (14) reduces to $\ddot{x} = -g\tan\theta$. The (x, θ) subsystem is

$$\ddot{x} = -g\tan\theta,$$
$$\ddot{\theta} = \tilde{\tau}_\theta.$$

Using a procedure similar to the one proposed for the roll control, we obtain

$$\tilde{\tau}_\theta = -\sigma_{\theta_1}\left(\dot{\theta} + \sigma_{\theta_2}\left(\theta + \dot{\theta} + \sigma_{\theta_3}\left(2\theta + \dot{\theta} - \frac{\dot{x}}{g} + \sigma_{\theta_4}\left(\dot{\theta} + 3\theta - 3\frac{\dot{x}}{g} - \frac{x}{g}\right)\right)\right)\right), \tag{21}$$

and thus θ, $\dot{\theta}$, x, and $\dot{x}$ also converge to zero.

Simulation Results

In this section, we compare the nonlinear control law (20) to a linear LQR controller. We focus our attention on the (y, ϕ) subsystem (18) and (19).

Define $\bar{x} = [y\ \dot{y}\ \phi\ \dot{\phi}]^T$. Then (18) and (19) can be rewritten as

$$\dot{\bar{x}} = A\bar{x} + B\bar{u}, \tag{22}$$

where

$$A = \begin{bmatrix} 0 & 1 & 0 & 0 \\ 0 & 0 & g & 0 \\ 0 & 0 & 0 & 1 \\ 0 & 0 & 0 & 0 \end{bmatrix}, \qquad B = \begin{bmatrix} 0 \\ 0 \\ 0 \\ 1 \end{bmatrix}, \bar{u} = \tilde{\tau}_\phi.$$

A state feedback control input is given by

$$\bar{u} = -K\bar{x}, \tag{23}$$

where $K = R^{-1}B^TP$, and P is the unique, positive-semidefinite solution to the algebraic Riccati equation. Using the control input (23) into (22), we obtain

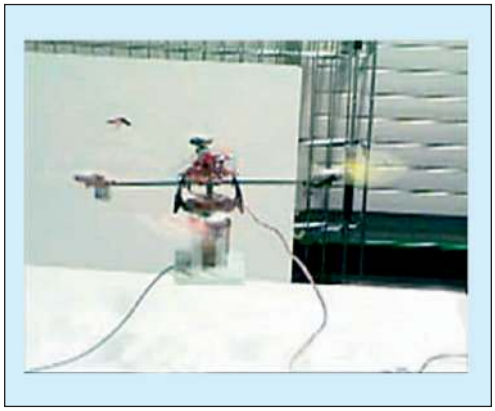

Figure 6. *Real-time quad-rotor control platform in autonomous hover. The control inputs are sent to the helicopter through a radio link. The wires attached to the rotorcraft provide connections to the power supply and the attitude sensor.*

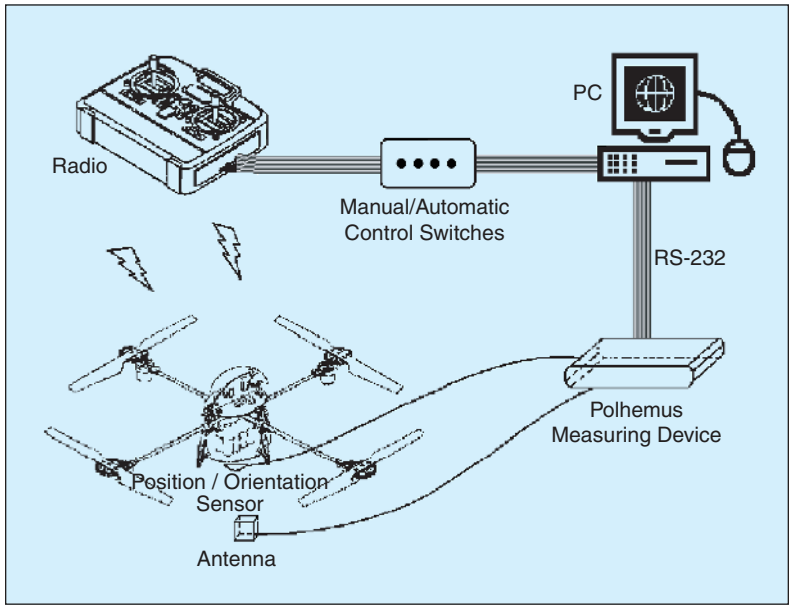

Figure 7. *Experimental setup. The position/orientation sensor on board the quad rotor is connected to a PC for feedback control. The PC generates control inputs, which are sent to the helicopter through the radio link.*

$$\dot{\bar{x}} = (A - BK)\bar{x}. \tag{24}$$

Choosing

$$Q = \begin{bmatrix} 1 & -2 & -4 & 6 \\ -2 & 4 & 8 & -12 \\ -4 & 8 & 16 & -24 \\ 6 & -12 & -24 & 36 \end{bmatrix}$$

and $R = 1$, the resulting gain that stabilizes system (24) is $K = [\,1 \quad 3.2848 \quad 29.3030 \quad 9.7266\,]$.

The closed-loop eigenvalues of $A - BK$ are -5.2393, -2.3946, -1.6056, and -0.4870, and thus the closed-loop system is asymptotically stable. Figure 2 shows the simulation results using the LQR control algorithm. The desired position is $\bar{x}_d = 0$. Note that for the initial conditions $y(0) = 70$ m, $\phi(0) = 0^\circ$, the state converges to zero.

Applying the LQR control law to the nonlinear system (10) and (15), and using the same conditions as before, the states y and ϕ diverge (see Figure 3). We observe in simulation that, for initial positions close to the desired position, the states converge to zero. However, if the rotorcraft is far from the desired position, the closed-loop system diverges (see Figure 3). This divergence is due to the fact that a large error in y produces a large angular displacement ϕ; therefore equation (18) is no longer an acceptable approximation for (15).

We now simulate the closed-loop system with the nonlinear control algorithm (20). We consider the initial conditions $y(0) = 5$ m and $\phi(0) = 17^\circ$. Figure 4 shows the simulation results for this subsystem (10) and (15) with the gains in Table 1. Note that $y \to 0$, $\dot{y} \to 0$, $\phi \to 0$, and $\dot{\phi} \to 0$. We observed that the speed of convergence increases as the amplitudes of the saturation functions increase. This trend is due to the fact that larger control inputs are allowed. Figure 5 shows similar results when the initial conditions are far from the desired position.

Simulation results show that, contrary to the LQR controller, the nonlinear controller in (20) stabilizes the equilibrium of subsystem (y, ϕ) around the origin for initial conditions far away from the desired position.

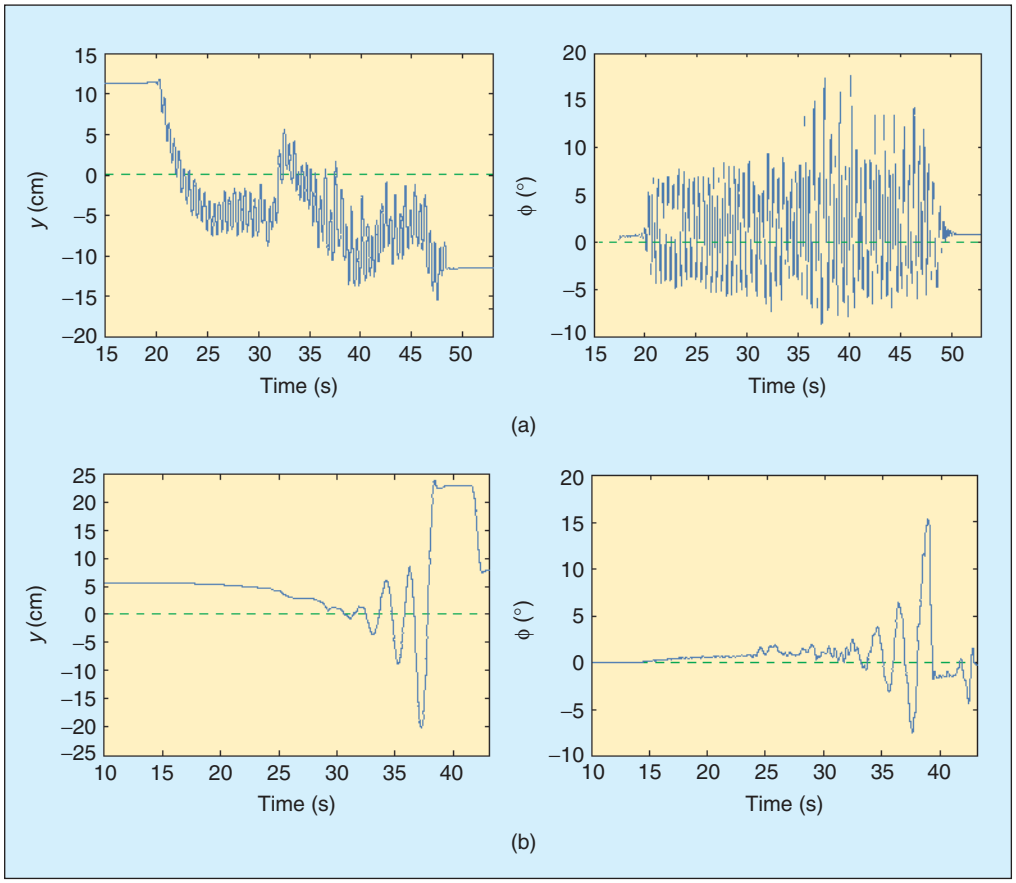

Figure 8. *Unstable response of the quad rotor for the LQR control law applied to the (ϕ, y) subsystem. (a) The dotted lines represent the desired trajectory for the initial conditions $y(0) = 12$ cm and $\phi(0) = 0^\circ$. The oscillations in the roll angle ϕ prevent the helicopter from taking off. In this experiment, we use the same controller parameters as in the simulation presented in Figure 2. (b) The LQR gains are manually adjusted to improve the performance of the mini rotorcraft, although the performance is inadequate for hovering.*

Experimental Results

Figure 6 shows the quad-rotor platform in autonomous hover. The experimental platform is composed of a Draganflyer helicopter, a Futaba 72-MHz radio, a Pentium II PC, and a 3-D tracker system (Polhemus) [11] for measuring the position (x, y, z) and orientation (ψ, θ, ϕ) of the quad rotor. The Polhemus is connected through an RS232 link to the PC (see Figure 7). The remote control system consists of a four-channel Futaba FM hobby radio.

An electronic circuit board in the helicopter contains three gyros, four pulsewidth modulation (PWM) speed controllers, a safety switch, and a microprocessor that mixes the pilot's commands to obtain the appropriate rotor control

inputs. The radio and the PC are connected using Advantech PCL-818HG and PCL-726 data-acquisition cards. To simplify the experiments, each control input is independently switched between automatic and manual control modes (see Figure 7).

The gyro stabilization introduces damping into the system and enables the quad rotor to be controlled manually. Without this gyro stabilization, it is almost impossible for a pilot to control the quad rotor manually [12], [13]. However, gyro stabilization, which represents only an angular speed feedback, is not sufficient for autonomous hover; for hover the quad rotor requires an attitude sensor, such as the Polhemus sensor, and a control law based on angular displacement feedback.

The control law requires the derivatives of the position (x, y, z) and the orientation (ψ, θ, ϕ). These derivatives are obtained numerically using the first-order approximation $\dot{q}(t) \approx (q(t) - q(t - T))/T$, where T is the sampling period. In all the experiments the position and orientation are provided by a Polhemus measuring device (see Figure 7).

LQR Control

Real-time experiments using the LQR control law are carried out with manual altitude control, that is, u is given by a pilot. To stabilize the system, we first implemented the LQR gains from the simulation results.

Figure 8(a) shows the lateral position and roll orientation of the quad rotor. As can be seen, the roll angle of the aircraft oscillates considerably, so that the helicopter cannot hover. To reduce the oscillations, we modify the gains to improve the performance. After numerous trials we significantly reduced the oscillations, as shown in Figure 8(b). Nevertheless, the obtained performance is not adequate to perform autonomous hovering.

Nonlinear Control Scheme

To apply the nonlinear control algorithm (20) to the rotorcraft, we place the aircraft in an arbitrary position, which is $(x, y, z) = (9, 12, 0)$ cm. The control objective is to make the rotorcraft hover at an altitude of 20 cm, that is, we

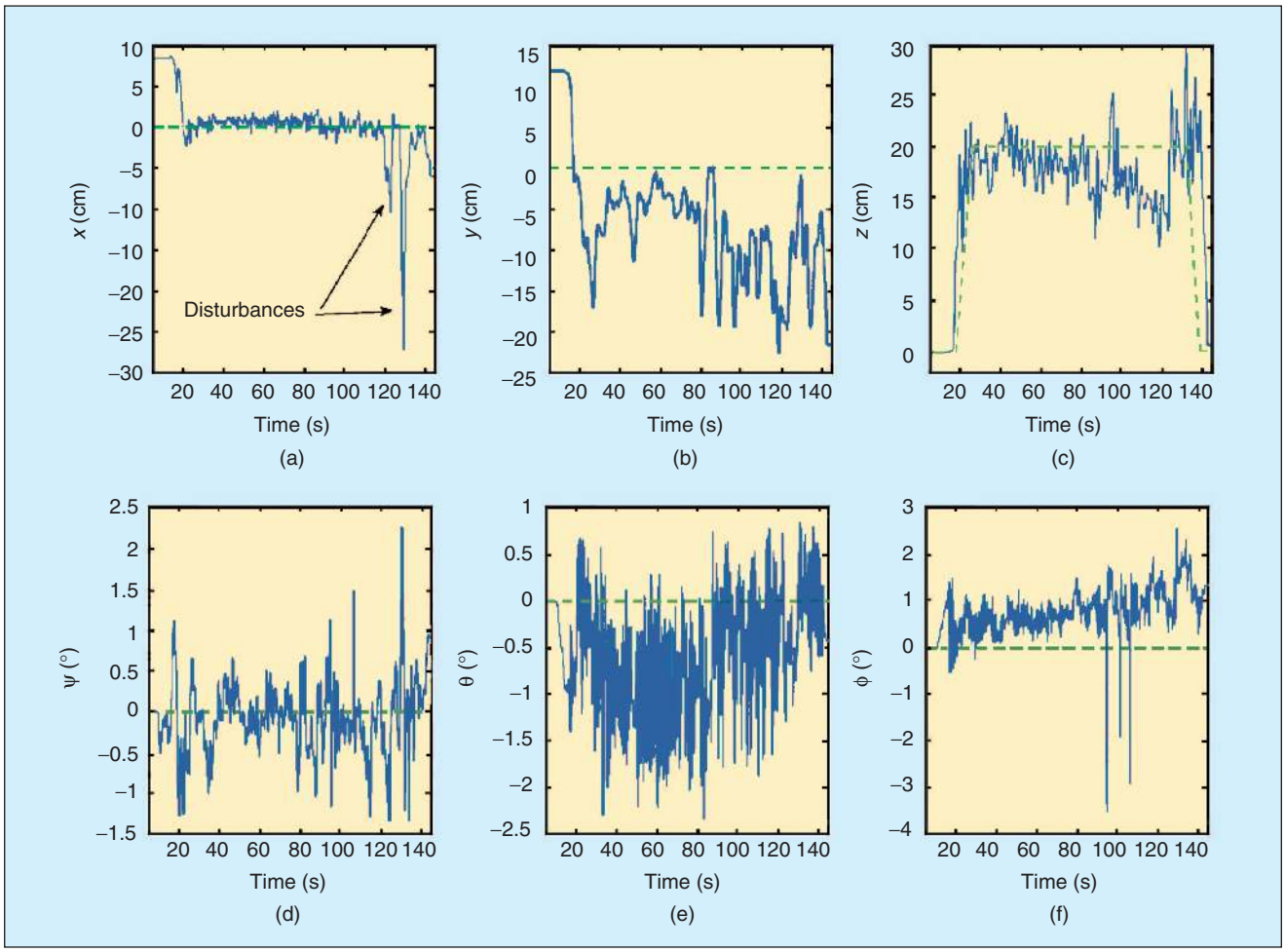

Figure 9. *Response of the quad rotor with position disturbances. The dotted lines represent the desired trajectory. The initial conditions are* $(x, y, z) = (8.7, 12, 0)$ *cm and* $(\psi, \theta, \phi) = (0^\circ, 0^\circ, 0^\circ)$. *The nonlinear controller recovers from position disturbances in x, y, and z introduced by pushing the quad rotor. The commanded hovering altitude is 20 cm.*

wish to reach the position $(x, y, z) = (0, 0, 20)$ cm while $(\psi, \theta, \phi) = (0^\circ, 0^\circ, 0^\circ)$, as shown in Figure 9. The controller parameters used in the experiment are given in Table 1. These parameters are tuned to obtain the best performance in practice.

The amplitudes of the saturation functions in the control law (20) are tuned as follows. We first tune the amplitude of σ_{ϕ_1} so that the roll angular velocity $\dot{\phi}$ remains close to zero even when a disturbance is introduced manually. We next select the amplitude of σ_{ϕ_2} in such a way that the quad-rotor roll angle is sufficiently small. In both cases, we avoid choosing high amplitude, which normally leads to oscillations. The amplitude of σ_{ϕ_3} is chosen so that the effect of a small disturbance in the horizontal speed $\dot{y}$ is soon compensated. Finally, the amplitude of σ_{ϕ_4} is chosen such that y is kept close to the desired position.

Figure 9 shows the performance obtained when we introduce a disturbance manually on the x-axis of -25 cm at time 125 s, five disturbances of -20 cm on the y–axis at times 25 s, 80 s, 90 s, 120 s, and 130 s, two disturbances of -10 cm on the z-axis at times 80 s and 115 s, and a disturbance of $+10$ cm on the z-axis at time 130 s.

We also study the system response to aggressive perturbations of the roll angle. In this experiment, we first apply a force manually to reach a roll angle of $+10^\circ$. At 95 s, we perturb the roll angle by -30°. As show in Figures 10 and 11, the response remains bounded.

Conclusions

We have presented a stabilization nonlinear control algorithm for a mini rotorcraft with four rotors. The dynamic model of the rotorcraft was obtained using a Lagrange approach. The proposed control algorithm is based on a

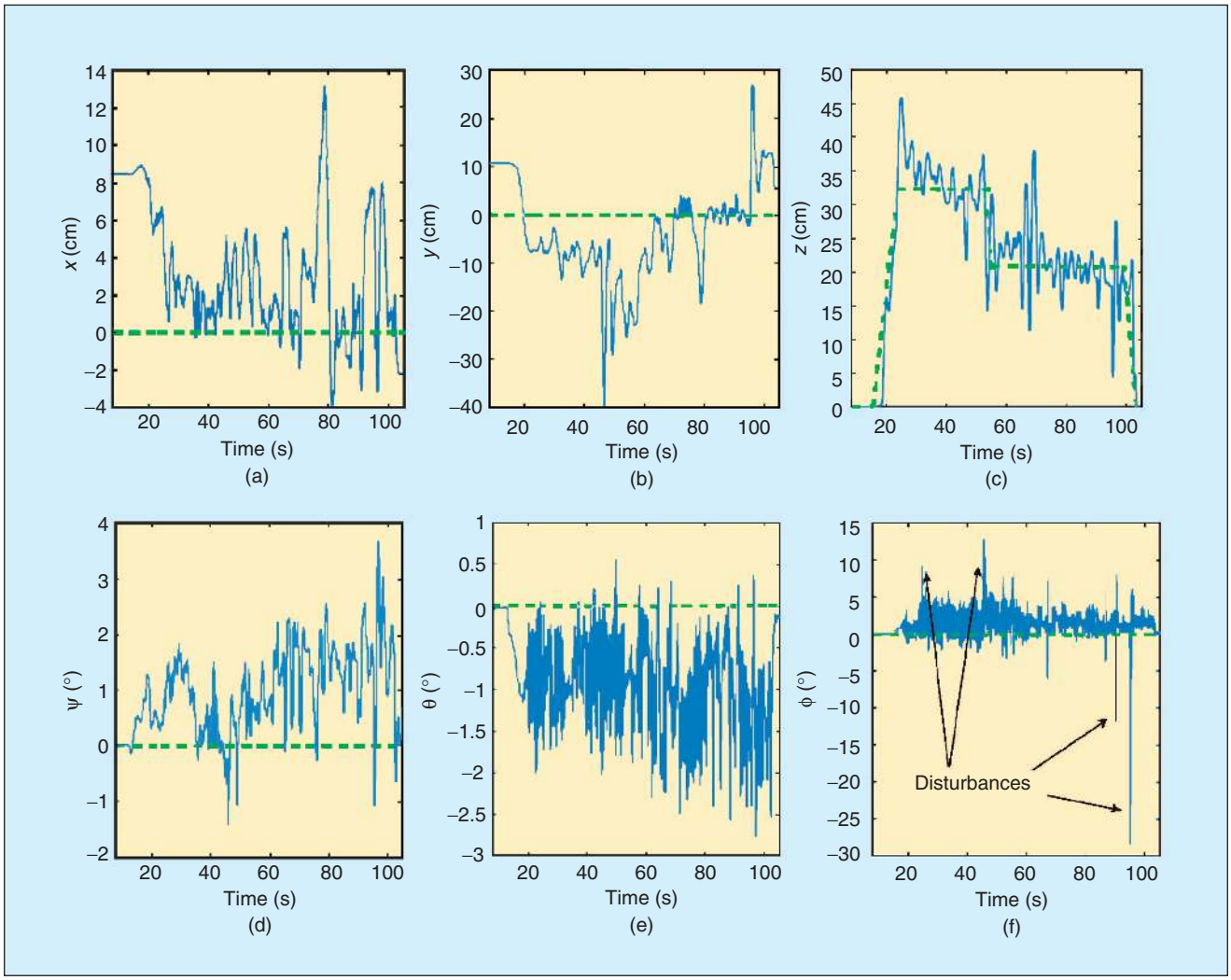

Figure 10. *Response of the quad rotor with roll disturbances. The initial conditions are* $(x, y, z) = (8, 12, 0)$ *cm and* $(\psi, \theta, \phi) = (0^\circ, 0^\circ, 0^\circ)$. *The dotted lines represent the desired setpoints. The roll angle* ϕ *is manually perturbed by* $+10^\circ$ *and* -30° *during the experiment. This experiment shows that the nonlinear control law can recover from large orientation perturbations.*

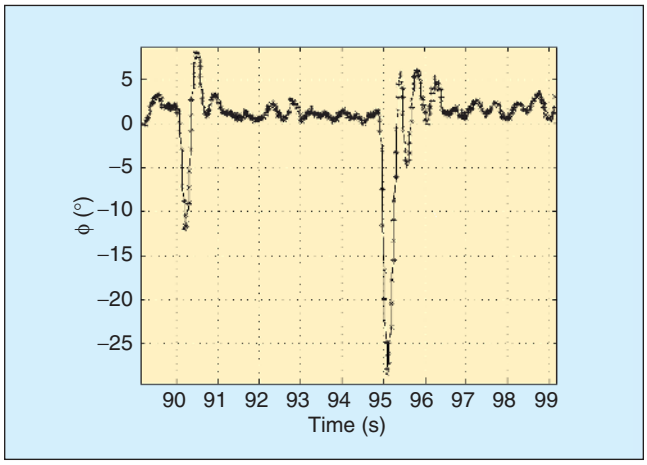

Figure 11. *System response to a roll angle perturbation. This closeup view corresponds to the roll angle in Figure 10. With the nonlinear control law, the subsystem (10) and (15) recovers from a roll perturbation of* -30°.

nested saturation control strategy, which is such that the amplitude constraints on the control input are satisfied.

The control strategy was applied to the mini rotorcraft, and the experimental results show that the controller performs satisfactorily even when significant disturbances are introduced into the system. Furthermore, experimental results show that the proposed nonlinear controller performs better than an LQR linear controller.

Acknowledgments

We are grateful for the financial support of the French Picardie Region Council, DGA, and LAFMAA (CNRS-CONACYT).

References

[1] V. Gavrilets, I. Martinos, B. Mettler, and E. Feron, "Control logic for automated aerobatic flight of miniature helicopter," in *Proc. AIAA,* Monterey, CA, Aug. 5–8, 2002, p. 4834.

[2] P. Castillo, R. Lozano, and A. Dzul, *Modelling and Control of Mini-Flying Machines* (Springer-Verlag Series in Advances in Industrial Control). New York: Springer-Verlag, 2005.

[3] I. Fantoni and R. Lozano, *Control of Nonlinear Mechanical Underactuated Systems (*Communications and Control Engineering Series). New York: Springer-Verlag, 2001.

[4] L. Marconi, A. Isidori, and A. Serrani, "Autonomous vertical landing on an oscillating platform: An internal-model based approach," *Automatica*, vol. 38, no. 1, pp. 21–32, 2002.

[5] A.R. Teel, "Global stabilization and restricted tracking for multiple integrators with bounded controls," *Syst. Contr. Lett.*, vol. 18, no. 3, pp. 165–171, 1992.

[6] T.S. Alderete, "Simulator aero model implementation" [Online], NASA Ames Research Center, Moffett Field, CA. Available: http://www.simlabs.arc.nasa.gov/library_docs/rt_sim_docs/Toms.pdf

[7] B. Etkin and L. Duff Reid, *Dynamics of Flight*. New York: Wiley, 1959.

[8] B.W. McCormick, *Aerodynamics Aeronautics and Flight Mechanics*. New York: Wiley, 1995.

[9] H. Goldstein, *Classical Mechanics,* 2nd ed. (Addison Wesley Series in Physics). Reading, MA: Addison-Wesley, 1980.

[10] J. Hauser, S. Sastry, and G. Meyer, "Nonlinear control design for slightly nonminimum phase systems: Application to V/STOL aircraft," *Automatica*, vol. 28, no. 4, pp. 665–679, 1992.

[11] *Fastrack 3Space Polhemus User's Manual*, Polhemus, Colchester, VT, 2001.

[12] P. Wayner, "Gyroscopes that don't spin make it easy to hover," *NY Times*, Aug. 8, 2002 [Online]. Available: http://www.nytimes.com

[13] N. Sacco, "How the Draganflyer flies," *Rotory Mag.*, 2002 [Online]. Available: http://www.rctoys.com/pdf/draganflyer3_rotorymagazine. pdf

Pedro Castillo (castillo@hds.utc.fr) obtained the B.S. degree in electromechanical engineering in 1997 from the Instituto Tecnológico de Zacatepec, Morelos, Mexico. He received an M.Sc. degree in electrical engineering from the Centro de Investigación y de Estudios Avanzados (CINVESTAV), Mexico, in 2000, and a Ph.D. in automatic control from the University of Technology of Compiègne, France, in 2004. His research interests include real-time control applications, nonlinear dynamics and control, aerospace vehicles, vision, and underactuated mechanical systems. He can be contacted at Heudiasyc-UTC, UMR CNRS 6599, B.P. 20529, 60205 Compiègne, France.

Rogelio Lozano received the B.S. degree in electronic engineering from the National Polytechnic Institute of Mexico in 1975, the M.S. degree in electrical engineering from the Centro de Investigación y de Estudios Avanzados (CINVESTAV), Mexico, in 1977, and the Ph.D. in automatic control from Laboratoire d'Automatique de Grenoble, France, in 1981. He joined the Department of Electrical Engineering at the CINVESTAV, Mexico, in 1981, where he worked until 1989. He was head of the Section of Automatic Control from June 1985 to August 1987. He has held visiting positions at the University of Newcastle, Australia, NASA Langley Research Center, and Laboratoire d'Automatique de Grenoble, France. Since 1990, he has been CNRS research director at the University of Technology of Compiègne, France, and, since 1995, head of the CNRS Laboratory Heudiasyc (Heuristique et Diagnostic des Systèmes Complexes). His research interests are in adaptive control, passivity, nonlinear systems, underactuated mechanical systems, and autonomous helicopters.

Alejandro Dzul received his B.S. degree in electronic engineering in 1993 and his M.S. degree in electrical engineering in 1997, both from Instituto Tecnológico de La Laguna, Mexico. He received the Ph.D. in automatic control from Université de Technologie de Compiègne, France, in 2002. Since 2003, he has been a research professor in the Electrical and Electronic Engineering Department at Instituto Tecnológico de La Laguna. His current research interests are in nonlinear dynamics and control and real-time control with applications to aerospace vehicles.